Gan, Tian; Ding, Guochang; Zhi, Xiaojing; Fan, Lijun; Hou, Nianjun; Yao, Xueli; Li, Ping; Zhao, Yicheng; Li, Yongdan

A $LaNi_{0.9}Co_{0.1}O_3$ coated $Ce_{0.8}Sm_{0.2}O_{1.9}$ composite anode for solid oxide fuel cells fed with methanol

Published in:
Catalysis Today

DOI:
10.1016/j.cattod.2018.04.050

Published: 01/05/2019

Document Version
Peer-reviewed accepted author manuscript, also known as Final accepted manuscript or Post-print

Please cite the original version:
Gan, T., Ding, G., Zhi, X., Fan, L., Hou, N., Yao, X., Li, P., Zhao, Y., & Li, Y. (2019). A $LaNi_{0.9}Co_{0.1}O_3$ coated $Ce_{0.8}Sm_{0.2}O_{1.9}$ composite anode for solid oxide fuel cells fed with methanol. *Catalysis Today*, *327*, 220-225. https://doi.org/10.1016/j.cattod.2018.04.050

A $LaNi_{0.9}Co_{0.1}O_3$ coated $Ce_{0.8}Sm_{0.2}O_{1.9}$ composite anode for solid oxide fuel cells fed with methanol

Tian Gan[1,2], Guochang Ding[1,2], Xiaojing Zhi[1,2], Lijun Fan[1,2], Nianjun Hou[1,2], Xueli Yao[1,2], Ping Li[1,2], Yicheng Zhao[1,2*], Yongdan Li[1,2,3*]

[1]State Key Laboratory of Chemical Engineering (Tianjin University), Tianjin Key Laboratory of Applied Catalysis Science and Technology, School of Chemical Engineering, Tianjin University, Tianjin 300072, China

[2]Collaborative Innovation Center of Chemical Science and Engineering (Tianjin), Tianjin, 300072, China.

[3]Department of Chemical and Metallurgical Engineering, Aalto University, Kemistintie 1, FI-00076 Aalto, Finland

Abstract

$Ce_{0.8}Sm_{0.2}O_{1.9}$ (SDC) powder is impregnated with $LaNi_{0.9}Co_{0.1}O_3$ (LNC) to form a composite anode for solid oxide fuel cells with methanol as fuel. Nanoparticles of Ni-Co alloy are derived from LNC after reduction. The composite anode shows a sufficient electrical conductivity when the weight ratio of Ni to SDC reaches 0.1, which is much lower than the amount of Ni required in conventional Ni-SDC anodes. The aggregation of Ni-Co nanoparticles in the reduced anode is suppressed by the oxide supporter, resulting in an improved catalytic activity. The single cell with LNC-SDC composite anode and SDC-carbonate composite electrolyte exhibits a maximum power density of 872 mW cm^{-2} at 700 °C with gasified methanol as the fuel, much higher than that of the

---

*Corresponding author. Email: zhaoyicheng@tju.edu.cn; Tel: +86-22-27405613; Fax: +86-22-27405243 (Y. Zhao)

*Corresponding author. Email: yongdan.li@aalto.fi, ydli@tju.edu.cn; Tel: +358-46-9214550 (Y. Li)

cell with a NiCo-SDC anode under the same condition. The amount of carbon deposited on the anode in methanol atmosphere decreases with the decline of the LNC content. The cells with LNC-SDC composite anodes exhibit stable performances during a 500-minute discharge period.

Keywords: Lanthanum nickelate; Impregnation; Anode; Solid oxide fuel cell; Methanol

1. Introduction

To meet the fast-growing demand for energy and solve the related environmental problems, intensive efforts have been dedicated to the design and development of advanced energy conversion devices [1-3]. Solid oxide fuel cells (SOFCs) are promising devices those convert chemical energy in fuels directly into electricity with a high efficiency [4, 5]. Anodes of SOFCs catalyze the oxidation of fuels and provide paths for oxygen ions and electrons [6]. The most common anode of SOFCs consists of metallic Ni as the catalyst and electronic conductor and a ceramic phase as the oxygen ionic conductor. In these anode, the content of each phase distributed randomly should exceed 30 vol% to reach the percolation threshold and form continuous conduction channels [7]. In practice, the content of Ni is usually higher than 45 vol% to achieve a sufficient electronic conductivity [8]. However, such a high amount of Ni suffers from not only aggregation at a high temperature, which results in the reduction of active sizes and the catalytic activity [9, 10], but also serious carbon deposition with hydrocarbons as fuels [11, 12]. Therefore, much attention has been focused on componential and structural modification of Ni-based cermet anodes [13, 14].

Impregnation technique is widely used in the preparation process of supported catalysts [15]. Catalytic active components are deposited on the inner surface of porous supporters. Consequently, a high active area could be obtained with a relatively low loading amount of active components [16]. In recent years, impregnation technique is used to fabricate electrodes of SOFCs [17, 18]. The components in electrodes made through impregnation are not randomly distributed, and a high electronic conductivity can be achieved with a low fraction of the conductive phase [19].

The exsolution of metallic nanoparticles from parent oxides in a reducing atmosphere provides another approach to produce catalysts with highly dispersed active components. The exsolution of some late transition metals, such as Ni, Fe and Co, from perovskites happens at a relatively high P_{O2} (10^{-4}-10^{-15} atm). The strong interaction between the oxide supporter and the metallic particles avoids the aggregation of these nanoparticles [20]. George et al. [21] utilized $La_{0.4}Sr_{0.4}Ni_{0.06}Ti_{0.94}O_{2.97}$ as the cathode material of a solid oxide electrolysis cell. The exsolution of metallic Ni in the 47% H_2O/3% H_2/50% N_2 atmosphere significantly improved the catalytic activity of the cathode for steam electrolysis. The exsolution strategy has been also used widely in the development of anode materials of SOFCs with H_2 as fuel [22-24].

Fuel flexibility is a major advantage of SOFCs over other types of fuel cells operated at a low temperature [25, 26]. Abundant and low-cost hydrocarbons could be utilized directly as fuels of SOFCs instead of pure H_2. However, severe carbon deposition happens on conventional Ni-based anodes in hydrocarbon atmospheres. Adding other metals in Ni to form alloys is an efficient way to improve the coking resistance of these anodes. Our previous works demonstrate that the formation of Ni-Mo and Ni-Co alloys could suppress carbon deposition in methanol atmosphere [27, 28]. Liu and coworkers [29, 30] found that Ni-Co alloy derived from hydroxides and perovskites exhibited high activity and good stability for methanation of CO and steam reforming of ethanol. In this work, $LaNi_{0.9}Co_{0.1}O_3$ (LNC)-$Ce_{0.8}Sm_{0.2}O_{1.9}$ (SDC) composite is synthesized by impregnation as the anode material of SOFCs. Ni-Co alloy formed after reduction acts as the active component and the electronic conductor. The performance of the anode is studied with methanol as fuel.

2. Experimental

2.1. Materials Preparation

SDC powder was synthesized through a hydrothermal procedure as described in previous works [31]. Stoichiometric $Ni(NO_3)_2{\cdot}6H_2O$, $Co(NO_3)_2{\cdot}6H_2O$ and $La(NO_3)_3{\cdot}6H_2O$ (99.5%, Guangfu fine chemical, Ltd., China) were dissolved in deionized water to form an aqueous solution with a total concentration of the metal ions of 0.3 mol L^{-1}. The solution was then impregnated into the SDC powder. The impregnated powder was dried at room temperature overnight and 100 °C for 12 h successively, and then sequentially calcined at 350 °C for 2 h and 800 °C for 5 h. The weight ratios of Ni to SDC in the anodes were 0.02:1, 0.10:1 and 0.20:1, which were referred to as 2LNC-SDC, 10LNC-SDC and 20LNC-SDC, respectively. The powders were reduced in hydrogen at 700 °C for 2 h for characterization.

For comparison, pure LNC powder was prepared with the sol-gel method as described elsewhere [32, 33]. Briefly, citric acid (99.5%, Guangfu fine chemical, Ltd., China) and ethylene glycol (Guangfu fine chemical, Ltd., China) were added to the aqueous solution used in the hydrothermal procedure mentioned above. The molar ratio of metal cations: citric acid: ethylene glycol was 1: 1.2: 0.24. Then the solution was continuously stirred at 80 °C until a gel was formed. The gel was dried at 120 °C for 12 h, and then calcined in air at 800 °C for 4 h to form the LNC powder.

A composite of 70 wt% SDC- 30 wt% $(Li_{0.67}Na_{0.33})_2CO_3$ was used as the electrolyte of the single cells. The cathode consisted of 30 wt% composite electrolyte and 70 wt% lithiated NiO. The synthesis procedures of the composite electrolyte and cathode materials were described in detail in previous works [34].

2.2. Characterization

The X-ray diffraction (XRD) patterns of the anode powders were recorded at room temperature using a D8 Focus diffractometer (Bruker Corp., Germany) with Cu-Kα radiation, 40 kV and 200 mA, at a scanning speed of 8° min^{-1}. The H_2 temperature programmed reduction (H_2-TPR) of the samples was carried out in 5% H_2-95% N_2 from room temperature to 800 °C at a heating rate of 10 °C min^{-1}. Transmission electron microscopy (TEM) images of the powders were observed with JEM 2100F electron microscope (JEOL, Japan) at 200 kV. The reduced anode powder was treated in gasified anhydrous methanol at 700 °C for 4 h. The carbon deposited was observed with a scanning electron microscope (SEM, Hitachi S-4800), and the weight of the carbon was measured with a PerkinElmer Diamond Thermogravimetric analyzer (TGA) in air from 30 to 1000 °C at a heating rate of 10 °C min^{-1}.

2.3. Performance of single cells

Electrolyte-cathode bilayers with a diameter of 13 mm were prepared through a co-pressing process at 500 MPa and then sintered at 700 °C in air for 1 h. The thicknesses of the electrolyte and the cathode layers were 0.50 and 0.35 mm, respectively. A slurry containing the anode powder and binder (V006, Heraeus Ltd.) was screen-printed on the electrolyte layer and then sintered at 700 °C in air for 1 h. The cross-sectional morphology of the single cell was studied with SEM. Ag paste was coated on both sides of the cell as a current collector.

The single cells were tested at 700 ºC with gasified anhydrous methanol (100 mL min^{-1}, STP) as the fuel and O_2 (30 mL min^{-1}, STP) as the oxidant, respectively, with an electrochemical workstation (VERSASTAT 3, Ametek). Before the test, the anode of the cell was reduced in H_2 at 700 ºC for 2 h. The electrochemical impedance spectra (EIS) of the cells were recorded under the open circuit voltage (OCV) in a frequency range from 1 M to 0.01 Hz with an amplitude of 10 mV. To evaluate the stability of the cells with methanol as fuel, the single cells were tested under a constant current density of 200 mA cm^{-2} at 700 ºC.

3. Results and discussion

3.1. Characterization

Pure LNC powder shows a perovskite structure which is in good accordance with the XRD pattern of $LaNiO_3$ (JCPDS#33-0711, Fig. 1a) [35, 36]. The peaks of SDC phase (JCPDS #073-1523) are observed in the XRD result of 2LNC-SDC without obvious LNC peaks probably due to the low amount of LNC phase. The LNC peaks become noticeable with the increase of the LNC content. No other peaks are shown in the patterns of the composites, implying that there is no interaction between SDC and LNC phases. The reduced LNC exhibits a mixed phase composed of La_2O_3 (JCPDS#54-0213), $La(OH)_3$ (JCPDS#36-1481) and Ni-Co alloy (Fig. 1b), which is also reported in previous works [37, 38]. The peaks of La_2O_3 and Ni-Co alloy phases are noticeable in the XRD profiles of reduced 10LNC-SDC and 20LNC-SDC composites.

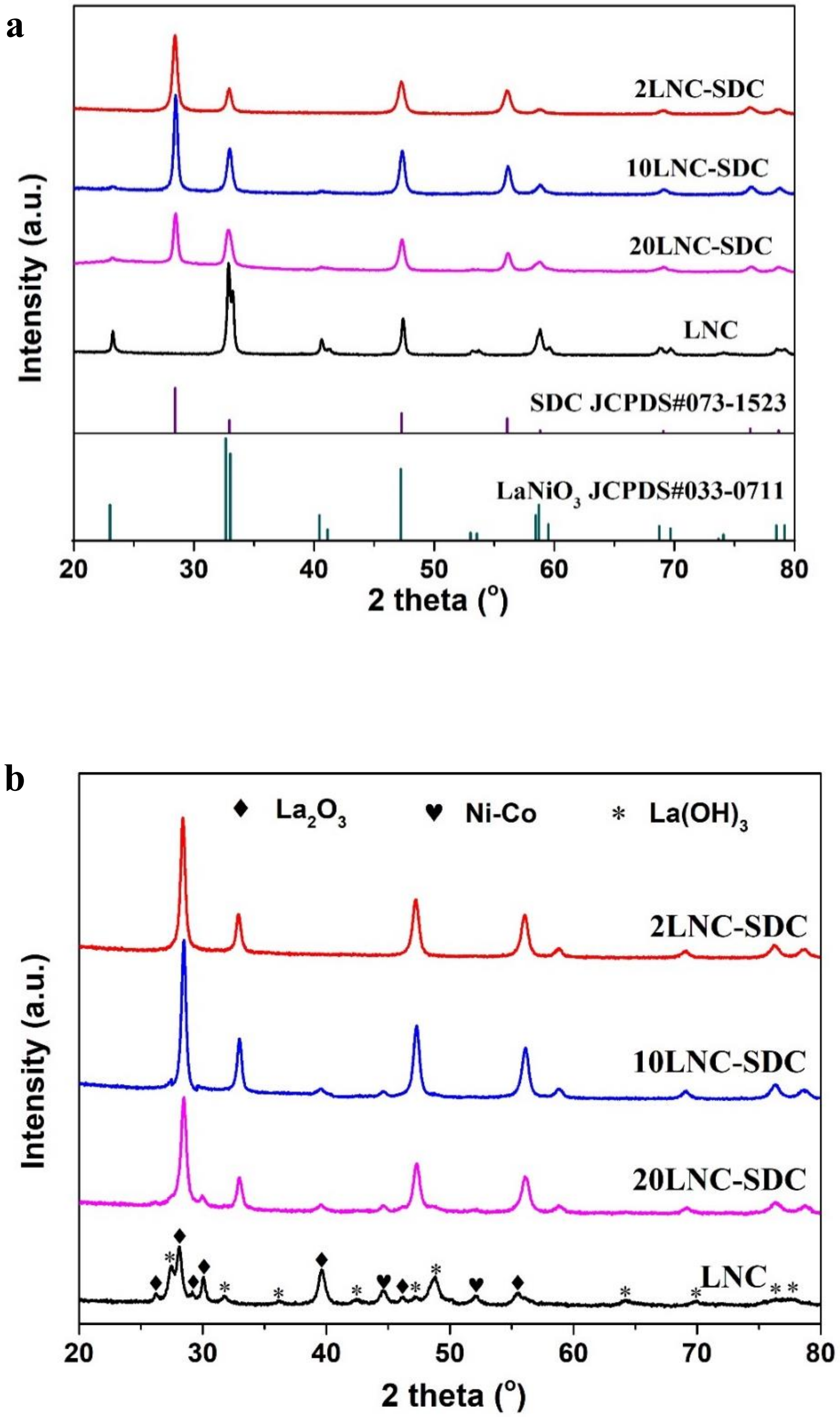

Fig. 1. XRD patterns of LNC-SDC powders (a) before and (b) after reduction

The H_2-TPR results of the anode powders are shown in Fig. 2. Pure SDC exhibits a weak reduction peak at about 495 °C. Two reduction peaks are observed in the result of pure LNC. The one in 200-380 °C is due to the reduction of Ni (III) and Co (III) to Ni (II) and Co (II) [39], while the other one in 430-560 °C corresponds to the reduction of Ni (II) and Co (II) to metallic Ni and Co [40]. Similar reduction processes of Ni (III) and Co (III) are observed in the H_2-TPR profiles of 10LNC-SDC and 20LNC-SDC composites. Meanwhile, another reduction peak in 170-260 °C appears in the results of the composite anodes, which could be ascribed to the reduction of adsorbed oxygen [41]. A few of Ce could diffuse into the LNC phase, leaving oxygen vacancies in the SDC phase. These oxygen vacancies facilitate the adsorption of oxygen species on the surface of SDC, which could be reduced by H_2 at a low temperature [20, 42].

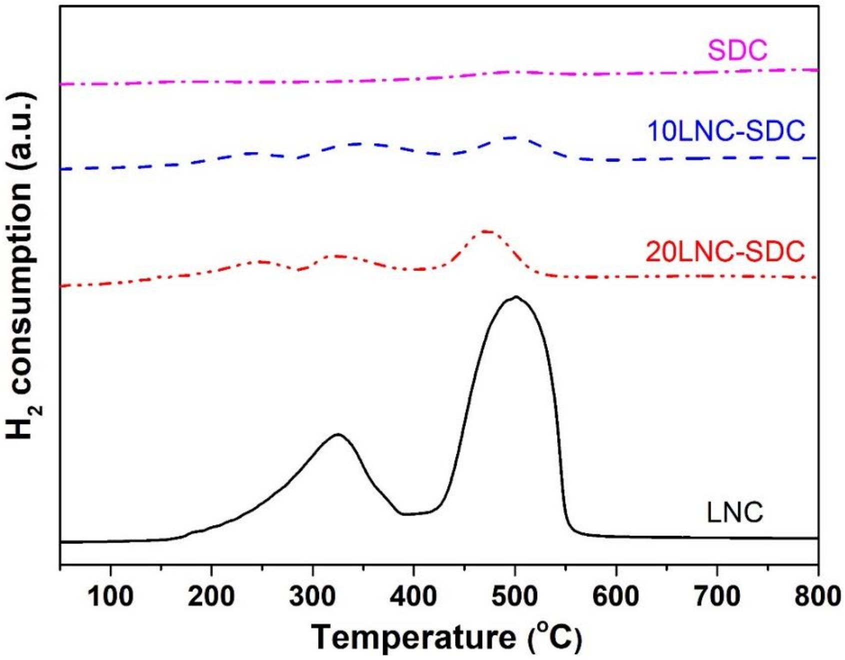

Fig. 2. H_2-TPR profiles of various powders

The TEM micrographs of the 10LNC-SDC powder before reduction are shown in Fig. 3a. The SDC particles with an average size of about 40 nm are covered by smaller

LNC particles with the size of 10-15 nm. The (200) lattice plane of SDC with an interplanar spacing of 2.71 Å and the (202) lattice plane of LNC with an interplanar spacing of 1.90 Å are observed in the high resolution TEM image of 10LNC-SDC (Fig. 3b). No obvious change in morphology is observed in the TEM result of the powder after reduction (Fig. 3c). Small particles with a spacing of 2.04 Å are on the surface of the SDC particles with a (111) plane and a spacing of 3.11 Å (Fig. 3d). It is known that the interspaces of Ni (111) and Co (111) planes are 2.037 and 2.046 Å, respectively [30]. Therefore, it is believed that the planes with a spacing of 2.04 Å correspond to the (111) plane of Ni-Co alloy [43].

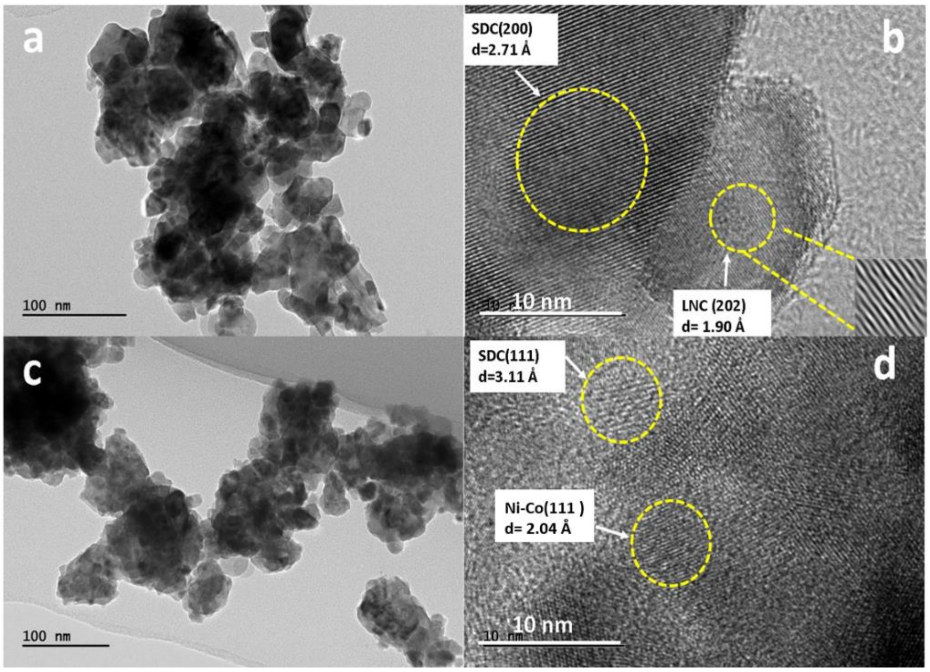

Fig. 3. TEM images of powders. (a) and (b) 10LNC-SDC before reduction; (c) and (d) 10LNC-SDC after reduction

3.2. Carbon deposition test

The SEM images of the reduced anode powders after carbon deposition are shown in Fig. 4. The carbon on the surface of 2LNC-SDC powder is negligible due to the low content of Ni. Obvious carbon whiskers are found on 10LNC-SDC powder. Carbon deposition becomes more serious with the increase of the amount of LNC, and pure LNC is completely covered by the deposited carbon.

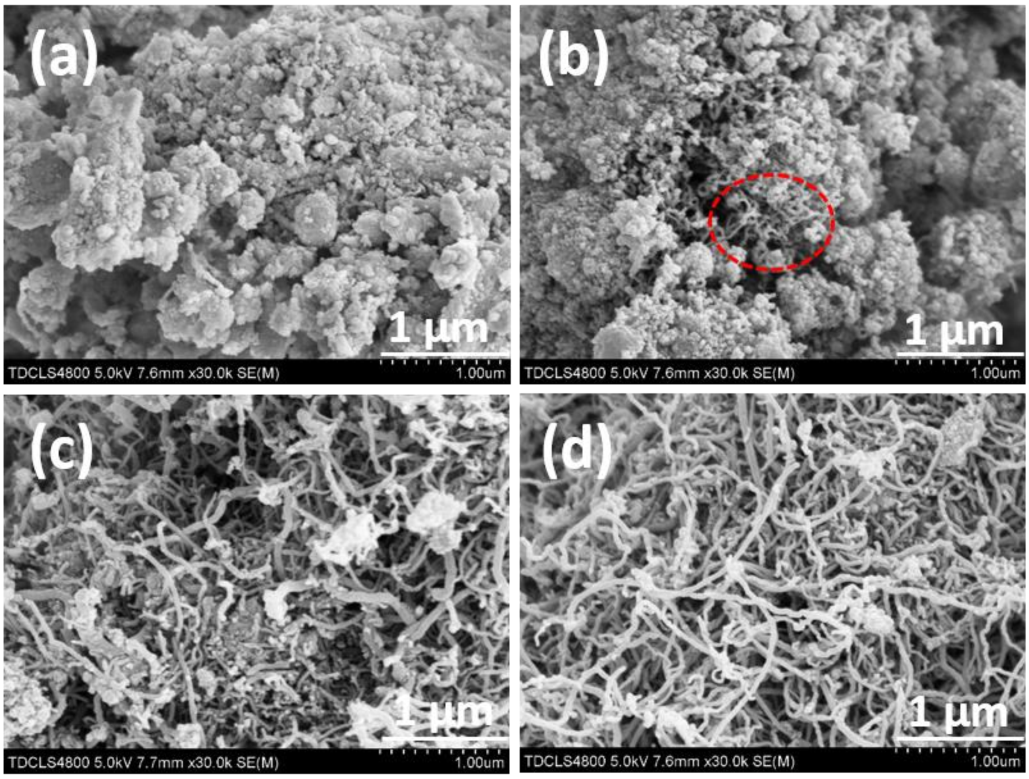

Fig. 4. SEM images of LNC-SDC powders after carbon deposition.

(a) 2LNC-SDC; (b) 10LNC-SDC; (c) 20LNC-SDC and (d) LNC.

The TGA curves of the reduced LNC-SDC powders after carbon deposition are exhibited in Fig. 5. The rapid weight loss of pure LNC starts at about 450 °C and finishes at about 680 °C. The weight loss of pure LNC is about 70% when the temperature reaches 1000 °C. The amount of deposited carbon reduces with the decrease of the content of LNC in the anode. The weight losses of 20LNC-SDC, 10LNC-SDC and 2LNC-SDC at 1000 °C are 42%, 14% and 5%, respectively. The TGA result of 70 mol% Ni$_{0.9}$Co$_{0.1}$-30 mol% SDC anode after carbon deposition, which is reported in our previous work [28], is also shown in Fig. 6 for comparison. The weight loss of the 70 mol% Ni$_{0.9}$Co$_{0.1}$-30 mol% SDC is about 43%, similar to that of the 20LNC-SDC powder. However, the rapid weight loss of 70 mol% Ni$_{0.9}$Co$_{0.1}$-30 mol% SDC starts at about 550 °C, which is approximately 150 °C higher than that of 20LNC-SDC, indicating that the carbon deposited on 20LNC-SDC is much easier to be oxidized.

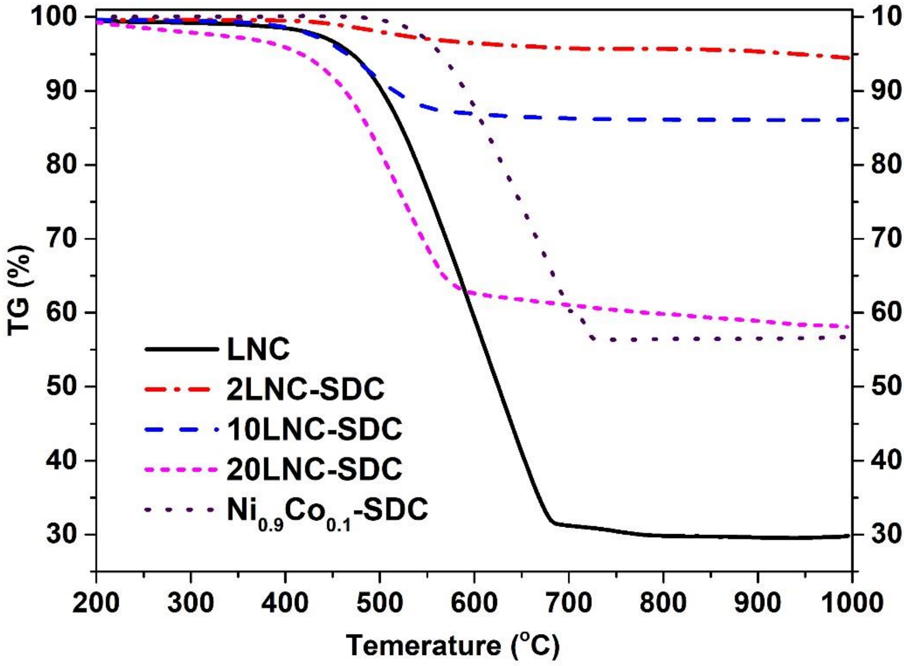

Fig. 5. TGA curves of LNC-SDC anodes after carbon deposition. The data of Ni$_{0.9}$Co$_{0.1}$-SDC come from ref. 28.

3.3. Cell performance

The cross-sectional morphology of the single cell with 10LNC-SDC anode is shown in Fig. 6. The thicknesses of the anode, electrolyte and cathode layers are 80, 500 and 350 μm, respectively. The anode and cathode layers adhere closely to the dense electrolyte layer with distinct interfaces. The porous structure of the electrode layers facilitates the diffusion of gaseous reactants and products and enlarges the reacting region.

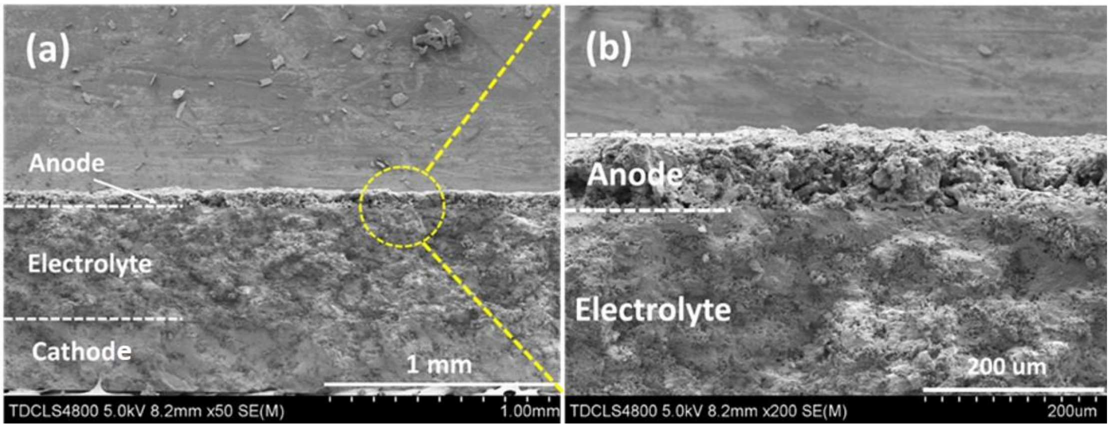

Fig. 6. Cross-sectional morphology of the single cell with 10LNC-SDC anode

Fig. 7a exhibits *I–V* and *I-P* characteristics of the single cells with various anodes at 700 °C. The open circuit voltage (OCV) of all the cells are around 1.15 V. The maximum output power densities ($P_{\max}$) of the cells with LNC, 2LNC-SDC, 10LNC-SDC and 20LNC-SDC as the anodes are 565, 453, 745 and 872 mW cm^{-2}, respectively. The EIS results of the single cells at 700 °C are shown in Fig. 7b. The high-frequency intercepts on the real axis reflect the ohmic resistances (R_{Ω}) of the cells and the arcs show the polarization resistances of the electrodes (R_{p}). Since the cathode and electrolyte are identical for all the cells, the differences of the R_{Ω} values are attributed to the variation of the conductivity of the anodes. The cell with 2LNC-SDC as the anode has the highest R_{Ω} of about 0.4 Ω cm^2. The amount of metal in the anode is too low to form continuous conductive pathways, leading to the high R_{Ω}. 2LNC-SDC anode also shows a high R_{p} due to the lack of active sites. Therefore, the cell with 2LNC-SDC anode exhibits the lowest $P_{\max}$. With the rise of the amount of metal in the anode layer, the electrical conductivity and catalytic activity of the anode both increase. A continuous layer of uniformly dispersed Ni particles might be formed on the surface of SDC when the content of Ni excesses 10%, and the R_{Ω} of the cells with 10LNC-SDC, 20LNC-SDC and pure LNC anodes are all around 0.3 Ω cm^2. 20LNC-SDC anode has the lowest R_p, and the cell with that anode shows the highest $P_{\max}$. Though pure LNC anode possesses more active sites than 20LNC-SDC, the anodic kinetics of LNC is limited by its low oxygen ionic conductivity. Therefore, the cell with pure LNC anode exhibits a high R_p and a low $P_{\max}$.

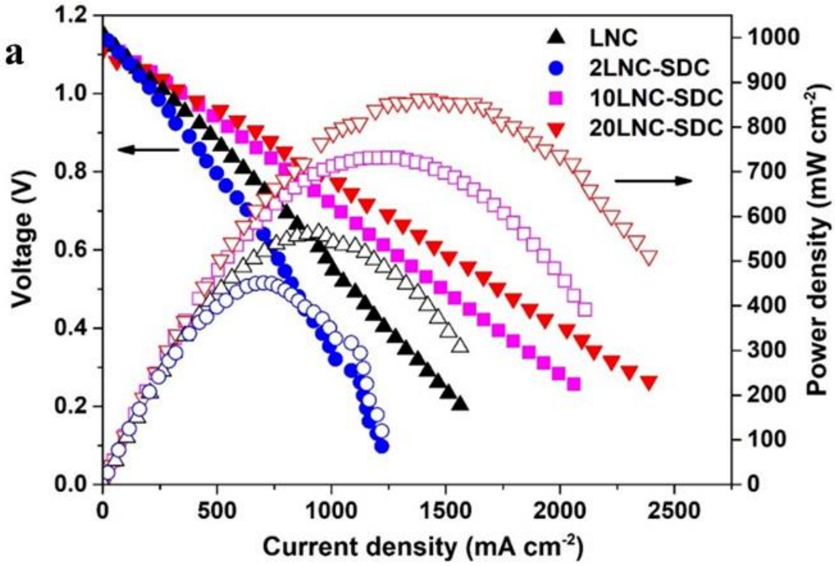

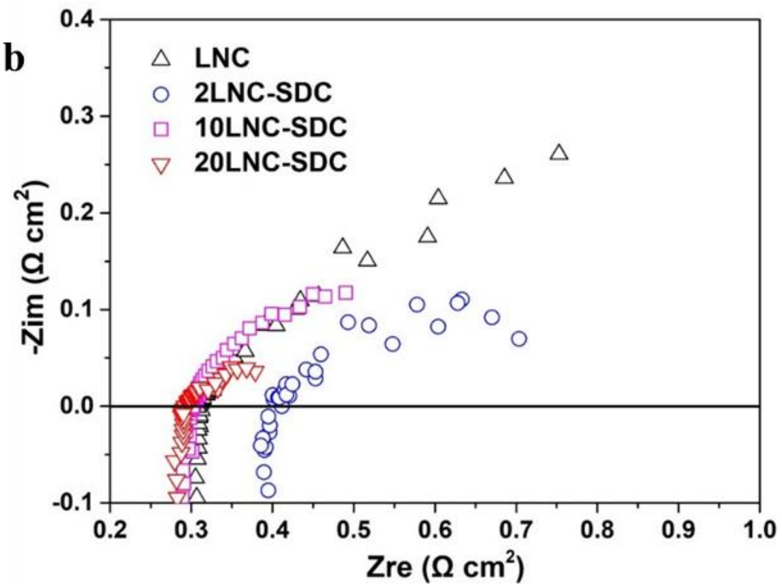

Fig. 7. (a) *I-V* and *I-P* curves and (b) impedance spectra of the fuel cells with LNC-SDC anodes at 700 °C with methanol as fuel.

As mentioned in the introduction, metal and oxide phases are distributed uniformly in conventional cermet anodes, and a high concentration of metal is required to form a continuous path for the conduction of electrons [45]. The content of Ni in most cermet anodes reaches 50 vol% and sometimes even 70 vol% to achieve the highest P_{max} [46]. The impregnation approach used in this work is an effective method to achieve a continuous metal phase and a sufficient electrical conductivity with a relatively low metal content. Furthermore, the aggregation of Ni-Co nanoparticles is hindered by the La_2O_3 phase [30, 47, 48]. The performances of the single cells with 20LNC-SDC and 70 mol% $Ni_{0.9}Co_{0.1}$-30 mol% SDC anodes (obtained from ref. [28]) are shown in Fig. 8. Compared with 70 mol% $Ni_{0.9}Co_{0.1}$-30 mol% SDC anode, 20LNC-SDC with a much lower content of NiCo exhibits a similar electrical conductivity and a quite low polarization resistance (Fig. 8a) due to the well distribution of catalytic nanoparticles.

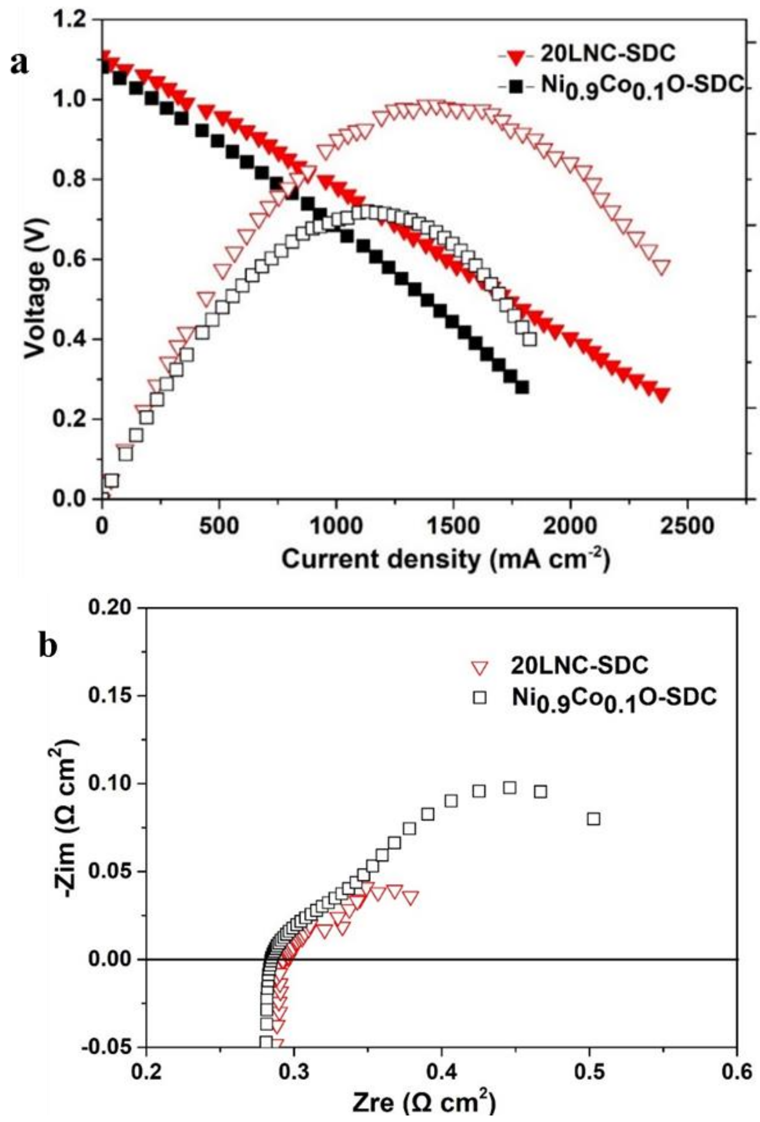

Fig. 8. (a) Impedance spectra and (b) *I-V* and *I-P* curves of the fuel cells with LNC-SDC and 70 mol% Ni$_{0.9}$Co$_{0.1}$O-30% mol% SDC anodes at 700 °C with methanol as fuel. The data of 70 mol% Ni$_{0.9}$Co$_{0.1}$O-30% mol% SDC come from ref. 28.

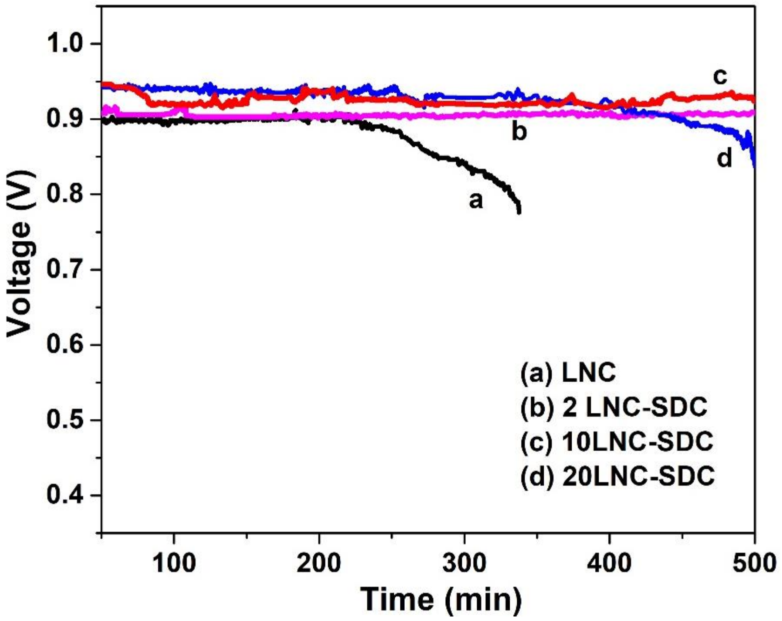

Fig. 9. Chronopotentiometry results of the single cells with various anodes under a current density of 200 mA cm^{-2} at 700 °C.

Fig. 9 shows the stability of the single cells with various anodes under a constant current density of 200 mA cm^{-2} at 700 ºC. The output voltage of the cell with the LNC anode remains stable at about 0.88 V during the first 220 min, and then drops gradually to 0.76 V within the next 115 min. The presence of SDC in the anode effectively suppresses the formation of carbon and leads to a higher stability of the single cells. The cell with 20LNC-SDC anode exhibits a stable output during the first 397 min, and then declines slowly. The cells with 2LNC-SDC and 10LNC-SDC anodes show stable performances during the 500-min discharge period, which is mainly due to the high resistance to carbon deposition of these anodes as proved by the TGA results. Meanwhile, the SDC phase with a high capacity to storage/release oxygen facilitates the electrochemical oxidation of both fuels and deposited carbon at the anode during the cell operation [37, 44], which could also improve the stability of the single cell.

4. Conclusions

The LNC coated SDC composite anode is synthesized by impregnation. LNC particles with the size of 10-15 nm on the surface of SDC particles form Ni-Co alloy after reduction. 2LNC-SDC anode shows a low electrical conductivity, while 10LNC-SDC presents a sufficient conductivity similar to that of pure LNC due to the continuous paths for electrons in the composite anode. 20LNC-SDC anode with good catalytic activity and oxygen ionic conductivity shows the lowest polarization with methanol as fuel. The single cell with that anode and SDC-$(Li_{0.67}Na_{0.33})_2CO_3$ composite electrolyte exhibits the highest $P_{\max}$ of 872 mW cm^{-2} at 700 ºC with methanol as fuel. LNC-SDC composite anode shows a high catalytic activity compared with conventional NiCo-SDC anode because the oxide supporter hinders the aggregation of metallic nanoparticles in the LNC-SDC anode. The carbon deposited in gasified methanol increases with the increase of the Ni content in the composite anode. Stable output performances are obtained by the cells with LNC-SDC composite anodes during the 500-min operation.

Acknowledgments

The financial support of NSF of China under contract number 51402210, the support of Tianjin Municipal Science and Technology Commission under contract number 15JCQNJC06500, and the support of the Ministry of Education of China under contract number 20130032120023 are gratefully acknowledged. The work has been also supported by the Program of Introducing Talents to the University Disciplines under file number B06006, and the Program for Changjiang Scholars and Innovative

Research Teams in Universities under file number IRT 0641.

References

[1] T. Guo, X. Dong, M.M. Shirolkar, X. Song, M. Wang, L. Zhang, M. Li, H. Wang, ACS Appl. Mater. Inter 6 (2014) 16131-16139.
[2] G. Corre, G. Kim, M. Cassidy, J.M. Vohs, R.J. Gorte, J.T.S. Irvine, Chem. Mater. 21 (2013) 1077-1084.
[3] Y. Wang, Z. Chen, H. Li, J. Zhang, X. Yan, K. Jiang, D.d. Engelsen, L. Ni, D. Xiang, Electrochim. Acta 222 (2016) 185-193.
[4] Z. Zhan, S.A. Barnett, Science 308 (2005) 844-847.
[5] H. Kan, H. Lee, Appl. Catal., B: Environ. 97 (2010) 108-114.
[6] S. Sengodan, Y.-W. Ju, O. Kwon, A. Jun, H.Y. Jeong, T. Ishihara, J. Shin, G. Kim, ACS Sustain. Chem. Eng. 5 (2017) 9207-9213.
[7] D.W. Dees, T.D. Claar, T.E. Easler, D.C. Fee, F.C. Mrazek, J. Electrochem. Soc. (1987) 2141-2146.
[8] A.A.A. da Silva, N. Bion, F. Epron, S. Baraka, F.C. Fonseca, R.C. Rabelo-Neto, L.V. Mattos, F.B. Noronha, Appl. Catal., B: Environ. 206 (2017) 626-641.
[9] R. Raza, Q. Liu, J. Nisar, X. Wang, Y. Ma, B. Zhu, Electrochem. Commun. 13 (2011) 917-920.
[10] E.D. Wachsman, T.L. Kang, Science 334 (2011) 935.
[11] B. Zhu, L. Fan, P. Lund, Appl. Energy. 106 (2013) 163-175.
[12] Y. Nabae, I. Yamanaka, M. Hatano, K. Otsuka, J. Phys. Chem. C 112 (2008) 10308-10315.
[13] J.R. Wilson, W. Kobsiriphat, R. Mendoza, H.Y. Chen, J.M. Hiller, D.J. Miller, K. Thornton, P.W. Voorhees, S.B. Adler, S.A. Barnett, Nat Mater 5 (2006) 541-544.
[14] W. Wang, C. Su, Y. Wu, R. Ran, Z. Shao, Chem. Rev. 113 (2013) 8104-8151.
[15] D.A. Osinkin, N.M. Bogdanovich, A.L. Gavrilyuk, Electrochim. Acta 199 (2016) 108-115.
[16] M. Lo Faro, D. La Rosa, I. Nicotera, V. Antonucci, A.S. Aricò, Electrochim. Acta 54 (2009) 5280-5285.
[17] D. Ding, X. Li, S.Y. Lai, K. Gerdes, M. Liu, Energ. Environ. SCI. 7 (2014) 552.
[18] S.P. Jiang, Mater. Sci. Eng., A 418 (2006) 199-210.
[19] J.M. Vohs, R.J. Gorte, Adv. Mater. 21 (2009) 943-956.
[20] M. Peymani, S.M. Alavi, M. Rezaei, Int. J. Hydrogen Energy 41 (2016) 6316-6325.
[21] G. Tsekouras, D. Neagu, J.T.S. Irvine, Energy Environ. Sci. 6 (2013) 256-266.
[22] J. Li, Y. Yu, Y.-M. Yin, N. Zhou, Z.-F. Ma, Electrochim. Acta 235 (2017) 317-322.
[23] Z. Du, H. Zhao, S. Yi, Q. Xia, Y. Gong, Y. Zhang, X. Cheng, Y. Li, L. Gu, K. Swierczek, ACS Nano 10 (2016) 8660-8669.
[24] Y. Gao, D. Chen, M. Saccoccio, Z. Lu, F. Ciucci, Nano Energy 27 (2016) 499-508.
[25] B. Hua, N. Yan, M. Li, Y.F. Sun, Y.Q. Zhang, J. Li, T. Etsell, P. Sarkar, J.L. Luo, Adv. Mater. 28 (2016) 8922-8926.

[26] M. Cimenti, J.M. Hill, J. Power Sources 195 (2010) 54-61.
[27] P. Li, B. Yu, J. Li, X. Yao, Y. Zhao, Y. Li, J. Power Sources 320 (2016) 251-256.
[28] G. Ding, T. Gan, J. Yu, P. Li, X. Yao, N. Hou, L. Fan, Y. Zhao, Y. Li, Catal. Today 298 (2017) 250-257.
[29] J. Liu, A. Cao, J. Si, L. Zhang, Q. Hao, Y. Liu, Nano 11 (2016) 1650118.
[30] L. Zhao, T. Han, H. Wang, L. Zhang, Y. Liu, Appl. Catal., B: Environ. 187 (2016) 19-29.
[31] L.M.P. Garcia, D.A. Macedo, G.L. Souza, F.V. Motta, C.A. Paskocimas, R.M. Nascimento, Ceram. Int. 39 (2013) 8385-8392.
[32] W. Wang, C. Su, R. Ran, Z. Shao, J. Power Sources 196 (2011) 3855-3862.
[33] N.T.Q. Nguyen, T.A. Trieu, H.H. Yoon, J. Electroceram. 35 (2015) 75-80.
[34] X. Dong, L. Tian, J. Li, Y. Zhao, Y. Tian, Y. Li, J. Power Sources 249 (2014) 270-276.
[35] S.M. Lima, J.M. Assaf, M.A. Peña, J.L.G. Fierro, Appl. Catal. A: Gen 311 (2006) 94-104.
[36] H. Zhu, W. Wang, R. Ran, Z. Shao, Int. J. Hydrogen Energy 38 (2013) 3741-3749.
[37] V. La Parola, G. Pantaleo, F. Deganello, R. Bal, A.M. Venezia, Catal. Today (2017).
[38] G. Valderrama, A. Kiennemann, M.R. Goldwasser, J. Power Sources 195 (2010) 1765-1771.
[39] G.S. Gallego, C. Batiot-Dupeyrat, J. Barrault, E. Florez, F. Mondragón, Appl. Catal. A: Gen 334 (2008) 251-258.
[40] H. Chen, H. Yu, F. Peng, G. Yang, H. Wang, J. Yang, Y. Tang, Chem. Eng. J. 160 (2010) 333-339.
[41] H. Liang, Int. J. Hydrogen Energy 40 (2015) 13338-13343.
[42] M.D. Salazar-Villalpando, B. Reyes, Int. J. Hydrogen Energy 34 (2009) 9723-9729.
[43] M.J. Hu, B. Lin, S.H. Yu, Nano Res. 1 (2010) 303-313.
[44] L. Katta, P. Sudarsanam, G. Thrimurthulu, B.M. Reddy, Appl. Catal., B: Environ. 101 (2010) 101-108.
[45] H. Kim, C. Lu, W.L. Worrell, J.M. Vohs, R.J. Gorte, J. Electrochem. Soc. 149 (2002) A247.
[46] N. Mahato, A. Banerjee, A. Gupta, S. Omar, K. Balani, Prog. Mater Sci. 72 (2015) 141-337.
[47] A. Yan, M. Phongaksorn, D. Nativel, E. Croiset, J. Power Sources 210 (2012) 374-380.
[48] B. Tu, Y. Dong, B. Liu, M. Cheng, J. Power Sources 165 (2007) 120-124.